Progress In Electromagnetics Research B, Vol. 47, 297–313, 2013

AN EFFICIENT IMAGING APPROACH FOR TOPS SAR DATA FOCUSING BASED ON SCALED FOURIER TRANSFORM

Pingping Huang[1, *] and Wei Xu[2]

[1]College of Information Engineering, Inner Mongolia University of Technology, Hohhot 010051, China

[2]Department of Spaceborne Microwave Remote Sensing, Institute of Electronics, Chinese Academy of Sciences (IECAS), Beijing 100190, China

Abstract—This paper presents an efficient imaging algorithm for Terrain Observation by Progressive Scans (TOPS) mode SAR raw data focusing. First, the use of subaperture is adopted to overcome the aliased Doppler spectra due to progress azimuth beam scanning. Afterwards, range compression and range cell migration correction (RCMC) are individually implemented in each azimuth block with its individual Doppler centroid. After azimuth subaperture signal recombination, a new Doppler centroid varying rate is introduced to avoid the reconstructed Doppler spectra wrapping. Moreover, azimuth varying beam center time is removed by azimuth frequency scaling before the final azimuth spectrum analysis (SPECAN) step. Finally, the conventional Fourier transform (FT) is replaced by the scaled Fourier transform (SCFT) step to obtain the uniform azimuth space sampling interval. Since the proposed imaging algorithm is without any interpolations and azimuth data extension, it is highly efficient. Simulation results on point targets validate the proposed algorithm.

1. INTRODUCTION

Terrain Observation by Progressive Scans (TOPS) mode is a novel proposed imaging mode of the wide swath synthetic aperture radar (SAR) operation scheme for future spaceborne SAR missions [1–4]. It achieves wide swath imaging coverage by periodically switching antenna beam from subswath to subswath, similar to conventional

Received 18 August 2012, Accepted 26 December 2012, Scheduled 8 January 2013

* Corresponding author: Pingping Huang (dzspph@gmail.com).

ScanSAR. In azimuth, antenna beam is actively steered from aft to fore with the opposite direction to the spotlight case during the whole acquisition interval. Consequently, targets with different azimuth locations are illuminated by the completed azimuth antenna pattern (AAP). The primary drawbacks in conventional ScanSAR, which are variations of azimuth ambiguity to signal ratio (AASR) and signal to noise ratio (SNR) along azimuth within the processed burst images, as well as scalloping effect, are obviously reduced and overcome [4–7]. The TOPS mode was firstly achieved by the TerraSAR-X satellite and has been chosen as the default mode of the European Space Agency (ESA)'s Sentinel-1 system for its interferometric wide swath imaging [4–7].

In TOPS, azimuth beam is either mechanically or electronically scanned from aft to fore during the whole acquisition interval [8–10]. This special scheme leads to the seriously increased Doppler bandwidth of the imaged scene, the target dwell time reduction and the azimuth variant instantaneous Doppler centroid [12, 13]. Consequently, three major problems should be overcome: the aliased Doppler spectra, the large range cell migration (RCM) [14–17] and the focused SAR imaging back folding in azimuth. Compared to other solutions to overcome the aliased Doppler spectra, the use of subaperture is a simple and efficient method. Moreover, range compression and range cell migration correction (RCMC) could be individually performed in each azimuth data block. If the conventional matched Doppler filter is chosen to focus the resulting azimuth signal in TOPS, a large azimuth data extension for up-sampling or/and additional post-processing steps [18] to resolve the output SAR image back folding problem are required. These operations make SAR imaging algorithms less efficient and require more computer memory. Fortunately, the SAR raw data with azimuth varying Doppler centroid can be focused via the efficient spectrum analysis (SPECAN) operation [17, 19, 20]. According to special properties of the TOPS raw data, an efficient focusing algorithm, which takes advantage of the use of subaperture, and SPECAN, is proposed. Moreover, azimuth scaling operations in the both time and Doppler domains are taken before the final SPECAN operation to avoid azimuth data wrapping. Simulation results on point targets validate the proposed algorithm.

This paper is organized as follows. Section 2 reviews the imaging geometry of the TOPS mode and analysis its corresponding raw data properties, especially in azimuth. Section 3 is focused on presenting the proposed imaging algorithm. Section 4 presents simulation results on point targets to validate the proposed approach. Finally, this paper is concluded in Section 5.

2. TOPS IMAGING MODE

In this section, the novel spaceborne TOPS imaging mode is reviewed, and properties of its corresponding echo signal especially in azimuth are analyzed.

2.1. Acquisition Geometry

Similar to conventional ScanSAR, the antenna elevation beam is periodically switched from subswath to subswath to achieve wide swath coverage illumination. To overcome primary disadvantages in ScanSAR, progressive azimuth beam scanning is introduced to shrink the AAP, and each target will be illuminated by the completed and reduced AAP. This scheme is usually achieved by electronically steering azimuth beam from aft to fore opposite to the spotlight mode via a planar phased antenna, as shown in Figure 1(a). However, since the antenna gain is symmetric, azimuth beam can also be actively steered as the same direction in the spotlight mode but at a higher rotation rate to shrink the AAP, as shown in Figure 1(b). Similar to the spotlight mode [12, 13], there is a fixed virtual rotation center during azimuth beam steering, as shown in Figure 1. In the figure, P is a point target with the position (x, r) in an imaged subswath, v_s and v_f indicate the effective velocities of the SAR sensor and the footprint, respectively, ω_r is the azimuth beam rotation rate, and r_{rot} is the slant range from the SAR sensor to the virtual rotation center. Assuming that the azimuth beam steering direction from aft to fore is positive, progressive azimuth beam steering introduces an azimuth shrinking factor, which

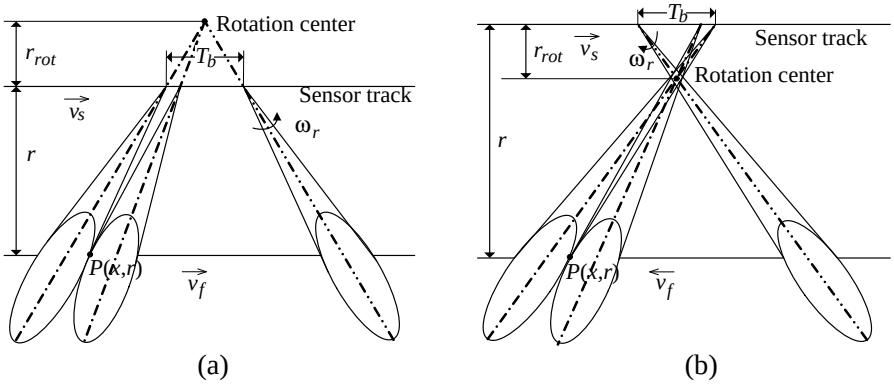

Figure 1. Planar TOPS mode imaging geometry in a subswath. (a) Nominal TOPS mode. (b) Inverse TOPS mode.

is response for the reduced target Doppler bandwidth and the coaster azimuth resolution. The shrinking factor is as follows [1]:

$$A(r) = \left| 1 + \frac{\omega_r r}{v_s} \right| \tag{1}$$

As a result, in TOPS, the obtained azimuth resolution in the near range is greater than in the far range. Since azimuth beam is steered from fore to aft in the inverse TOPS mode, it requires the higher rotation rate than the nominal TOPS mode for the same achieved azimuth resolution, and the higher rotation rate ω_{ir} can be expressed as:

$$\omega_{ir} = -\left(\frac{2v_s}{r} + \omega_r \right) \tag{2}$$

From both imaging geometries in Figure 1, the slant range r_{rot} from the SAR sensor to the virtual rotation center can be easily obtained as follows:

$$r_{rot} = -v_s/\omega_r \tag{3}$$

Moreover, targets with different azimuth locations are illuminated with different squint angles due to azimuth beam steering during the whole acquisition interval, this scheme introduces an instantaneous Doppler centroid varying rate given by [1]:

$$k_{rot} = \frac{\partial f_{dc}(t)}{\partial t} = \frac{2v_s\omega_r}{\lambda} = -\frac{2v_s^2}{\lambda r_{rot}} \tag{4}$$

where f_{dc} is the instantaneous Doppler centroid.

2.2. Properties of Azimuth Signal in TOPS

The difference of the TOPS SAR signal is its corresponding azimuth signal component due to progressive azimuth beam scanning with the opposite direction to the traditional spotlight mode. Moreover, the maximum azimuth steering angle adopted in the spaceborne TOPS mode is quite limited, e.g., $\pm 0.75^\circ$ in the TerraSAR-X satellite and $\pm 0.7^\circ$ in the Sentinel-1 SAR system [6]. Therefore, we just need to focus on analyzing properties of the TOPS SAR azimuth signal. The simplified expression of azimuth signal of point target $P(x, r)$ is:

$$s_a(\tau, t; x, r) = \text{rect}\left[\frac{t - x/v_f}{T_d} \right] \cdot \exp\left[-j\frac{4\pi}{\lambda} r \right] \cdot \exp\left[-j\frac{4\pi}{\lambda} \cdot \Delta R(t; x, r) \right] \tag{5}$$

with

$$\Delta R(t; x, r) \approx \frac{(v_s t - x)^2}{2r} \tag{6}$$

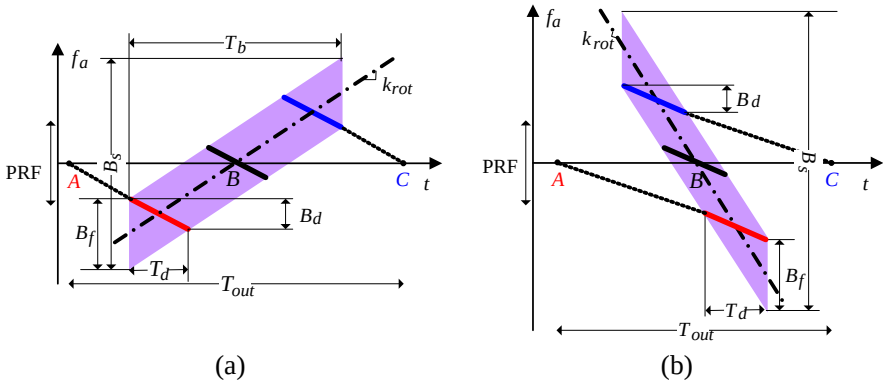

Figure 2. TOPS raw data supports in the slow time frequency domain (TFD). (a) Nominal TOPS mode. (b) Inverse TOPS mode.

where T_d is the target dwell time. Equation (6) neglects the higher order phase terms for the analysis simplify, and it will not affect the imaging algorithm quality, since the higher order terms are still compensated in the following proposed imaging algorithm. Afterwards, the Doppler spectrum of the point target P can be computed as follows:

$$S_a(f_a; x, r) = \exp\left(-j\frac{4\pi}{\lambda}r\right)\exp\left(-j\pi\frac{f_a^2}{k_a} - j2\pi f_a t_x\right) \operatorname{rect}\left[\frac{f_a + (A-1)k_a t_x/A}{B_d}\right] \tag{7}$$

with

$$k_a = -\frac{2v_s^2}{\lambda r} \tag{8}$$

where B_d is the point target Doppler bandwidth.

According to Equations (5) and (7), the raw data support in the slow time/frequency domain (TFD) is shown in Figure 2 for both TOPS modes. There are three imaged targets with the full azimuth resolution in the illuminated scene as shown in Figure 2. The total Doppler bandwidth of a single burst B_s and the target Doppler bandwidth B_d are expressed as follows:

$$B_s = |k_{rot}|\,T_b + B_f \tag{9}$$

$$B_d = B_f/A \tag{10}$$

where B_f is the azimuth beam bandwidth exploited for azimuth data focusing. It can be seen that the total Doppler bandwidth might span over several times PRF intervals due to progressive azimuth

beam scanning during the whole acquisition time, although the target Doppler bandwidth is reduced. Moreover, the total Doppler bandwidth in the inverse TOPS mode is larger than in the TOPS mode due to its higher rotation rate for the same azimuth resolution.

As the large size of imaged scene in azimuth is illuminated in a short bust duration in TOPS, the required output duration in the azimuth time domain to avoid the output wrapping for both fully and partly focused targets is as follows:

$$T_{out} = B_s/|k_a| \tag{11}$$

However, the dwell time for each target in azimuth is reduced to:

$$T_d = T_f/A \tag{12}$$

where T_f is the whole synthetic aperture time in the stripmap case with the same azimuth beam angular interval.

Therefore, three major problems, which are the aliased Doppler spectra, the large range cell migration (RCM) and the output focused SAR image back folding in azimuth, should be resolved during TOPS SAR raw data focusing.

3. MODIFIED ECS ALGORITHM

In the SAR imaging algorithms, RCMC is the most important focusing step to deal with higher order range-azimuth coupling

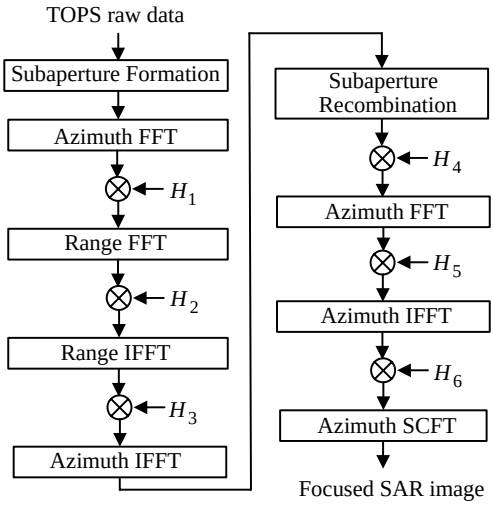

Figure 3. Block diagram of the proposed algorithm.

terms. Fortunately, the spaceborne TOPS mode usually has a limited maximum azimuth beam steering capability, and existing stripmap focusing processors [16–24] can implement SAR data focusing well in this case. In addition to taking conventional stripmap imaging processors, problems of the aliased Doppler spectra and the azimuth output back folding in the SAR image should be resolved. Therefore, additional pre-processing and post-processing steps are usually required to resolve these problems. Zan [1] presents a novel imaging approach for the TOPS raw data, and it makes use of additional steps by generalizing the mosaic approach formerly for spotlight SAR and ScanSAR [12, 18]. However, this approach is not very efficient due to the large required azimuth data extension. Baseband azimuth scaling (BAS) algorithm [5] is an efficient imaging approach for TOPS SAR data focusing. This paper presents another novel efficient phase preserving imaging algorithm for the TOPS raw data. The block diagram of the proposed modified extended chirp scaling (ECS) is shown in Figure 3. First, the whole burst raw data is divided into several blocks in azimuth to avoid the aliased Doppler spectra, and each block is individually processed via the classic chirp scaling (CS) algorithm according to its individual Doppler centroid. After azimuth data recombination, the modified SPECAN algorithm based on scaled Fourier transform (SCFT) is adopted to focus the azimuth signal.

3.1. Use of Subaperture

Progressive azimuth beam steering during the whole raw data acquisition time makes that the total Doppler bandwidth of a single burst may span over several pulse repetition frequency (PRF) intervals. In order to accommodate to the large Doppler bandwidth, several processing approaches [1, 5–10] have been proposed. The use of subaperture is a simple way to overcome this problem. To avoid the aliased Doppler spectrum in each block, the size of azimuth block is computed as follows:

$$T_{block} \leq \frac{\mathrm{PRF} - B_f}{k_{rot}} \tag{13}$$

After the azimuth data division into multiple blocks, each subaperture data is processed corresponding to its individual Doppler centroid. To achieve a smooth subaperture data recombination, the subaperture data should be formed with some overlap which is usually about 5%∼10% [5].

Classic chirp scaling algorithm is an efficient focusing algorithm to process the raw data with a low squint angle without any

interpolations. The steps of chirp scaling, RCMC, range compression are implemented by multiplying phase functions H_1 and H_2, while these functions can be found in [17]. The function H_3 is multiplied to compensate the phase error caused by the chirp and range scaling operation [17] and remove high order terms of each target Doppler history, and it can be expressed as:

$$H_3 = \exp\left[j\Delta\varphi + j\frac{4\pi r}{\lambda}\left(\beta(f_a) - 1\right) + j\frac{\pi\lambda r}{2v_s^2}f_a^2\right] \tag{14}$$

with

$$\beta(f_a) = \sqrt{1 - \left(\frac{\lambda f_a}{2v}\right)^2} \tag{15}$$

where $\Delta\varphi$ is the residual phase term which can be found in [17]. After the azimuth inverse fast Fourier transform (IFFT) to transform raw data back to the azimuth-range time domain, the azimuth data recombination is carried out.

3.2. Modified SPECAN Operation in Azimuth

However, after the subaperture data recombination, the total Doppler bandwidth still spans over multiple PRF intervals. Therefore, the high

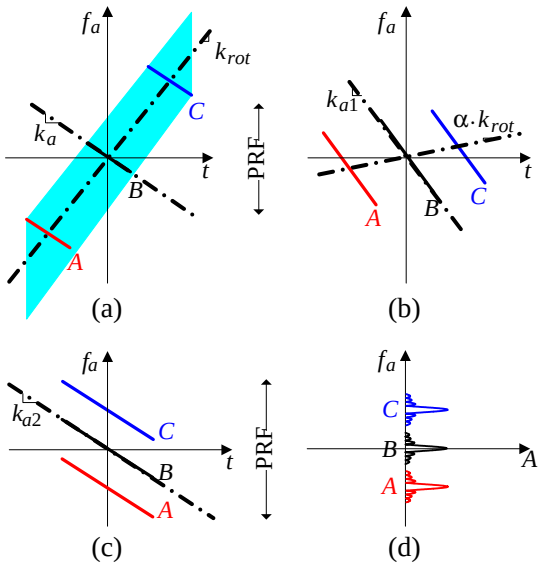

Figure 4. Graphic explanation of azimuth data focusing. (a) Original azimuth TFD support. (b) TFD after H_4. (c) TFD after H_5. (d) Frequency-amplitude diagram after H_6.

Doppler centroid varying rate should be replaced by a low varying rate via using the following phase function:

$$H_4 = \exp\left[-j\pi(1-\alpha)\cdot k_{rot}(t-t_{mid})^2\right] \tag{16}$$

where t_{mid} is the bust center time, and $0 < \alpha < 1$ is a constant scaling factor. Moreover, the residual Doppler centroid varying rate is still remained as shown in Figure 4(b). To avoid the aliased Doppler spectra, the constant value α should be

$$\alpha \leq \frac{\mathrm{PRF} - B_{d1}(r_0)}{|k_{rot}|\cdot T_b} \tag{17}$$

where B_{d1} is the new target Doppler bandwidth, and r_0 is the slant range from the imaged scene center to the SAR sensor. Furthermore, azimuth data filtering in the first and last subaperture should be carried out to reduce the effective Doppler bandwidth. Afterwards, the new Doppler modulation rate k_{a1} and the new Doppler bandwidth B_{d1} of point target can be respectively expressed as:

$$k_{a1} = k_a - (1-\alpha)k_{rot} = -\frac{2v^2}{\lambda}\cdot\frac{r_{rot}+r-\alpha\cdot r}{r\cdot r_{rot}} \tag{18}$$

$$B_{d1} = \frac{B_f}{A}\cdot\left|\frac{k_{a1}}{k_a}\right| \tag{19}$$

Before the final azimuth SPECAN operation, the azimuth scaling phase function is multiplied to remove the azimuth varying beam center time. From Equation (16), this phase function is obtained as follows:

$$H_5 = \exp\left[-j\pi\frac{f_a^2}{\alpha\cdot k_{rot}}\right] \tag{20}$$

Different from azimuth scaling in [17] to remove the target original Doppler histories and introduce a constant linear frequency modulation rate, targets with different slant ranges still have different azimuth modulation rates. Moreover, this step doesn't require any azimuth data extensions to avoid wrap effects in the burst signal after azimuth scaling. Consequently, the target Doppler modulation rate becomes

$$k_{a2} = \left(\frac{1}{k_{a1}} - \frac{1}{\alpha\cdot k_{rot}}\right)^{-1} = -\frac{2v^2}{\lambda}\cdot\frac{\alpha(r_{rot}+r-\alpha r)}{r_{rot}(r_{rot}+r)} \tag{21}$$

Afterwards, the new target dwell time is extended to

$$T_{d\_new} = -\frac{B_{d1}}{k_{a2}} = \frac{B_f}{A}\cdot\left|\frac{k_{a1}}{k_a\cdot k_{a2}}\right| = \frac{T_f}{A-1}\cdot\frac{1}{\alpha} \tag{22}$$

If the factor α makes the new target dwell time T_{d_new} exceed the burst duration T_b, azimuth data extension is required. This is also the reason

that the Doppler filtering is taken in the first and last subaperture before azimuth data recombination.

After multiplying the function H_5, the TOPS raw data can be expressed as follow:

$$\begin{aligned} S_5(\tau, f_a) \;=\; & C \cdot \mathrm{sinc}\left[\pi K_r \tau_p \left(\tau - \frac{2r}{c}\right)\right] \exp\left[-j\frac{4\pi r}{\lambda}\right] \\ & \exp\left[-j\pi\frac{f_a^2}{k_{a2}} - j2\pi f_a \frac{x}{v}\right] \end{aligned} \tag{23}$$

where C is a constant, K_r and τ_p indicate the modulation rate of the transmitted chirp signal, respectively, τ is the fast time, and c is the light speed. According to Equation (23), the deramping function to compensate the linear frequency is as:

$$H_6 = \exp\left[-j\pi k_{a2}(t - t_{mid})^2\right] \tag{24}$$

If the conventional Fourier transform is introduced to compress the resulting azimuth signal, the obtained focused TOPS in the range-Doppler domain is as follows:

$$\begin{aligned} S_6(\tau, f_a) &= FT\{s_5(\tau, t) \cdot H_6\} \\ &= C_1 \cdot \mathrm{sinc}\left[\pi K_r \tau_p \left(\tau - \frac{2r}{c}\right)\right] \\ &\quad \mathrm{sinc}\left[\pi \Delta t' \cdot N_{fft}\left(f_a - \frac{2v^2}{\lambda} \cdot \frac{\alpha(r_{rot}+r-\alpha r)}{r_{rot}(r_{rot}+r)} \cdot \frac{x}{v}\right)\right] \end{aligned} \tag{25}$$

where $FT\{\cdot\}$ is the Fourier transform operator, $s_5(\tau, t)$ is the raw data of $S_5(\tau, f_a)$ in the 2D (two dimension) time domain, $\Delta t' = 1/\mathrm{PRF}$ is the azimuth signal sampling interval, and N_{fft} is the number of the azimuth samples used for the azimuth fast Fourier transform (FFT). Consequently, the obtained output azimuth space sampling interval can be computed as follows:

$$\Delta x = \frac{1}{\Delta t' \cdot N_{fft}} \cdot \frac{\lambda}{2v} \cdot \frac{r_{rot}(r_{rot}+r)}{\alpha(r_{rot}+r-\alpha r)} \tag{26}$$

It can be seen that the space sampling interval Δx depends on the range bin, which means that the final TOPS mode SAR images requires additional resampling for azimuth geometric correction. ECS algorithm in [17] can obtain the uniform azimuth space sampling interval by removing the target original range dependent history and introducing a constant frequency modulation rate. However, this imaging algorithm requires the azimuth data extension in the time domain to avoid the azimuth wrap effect. To avoid the additional resampling for azimuth geometric correction, the scaled

Fourier transform (SCFT) is replaced by the conventional Fourier transform, which is formerly proposed for ScanSAR data focusing in [20]. In this algorithm, the kernel of the adopted SCFT operator is different from the kernel for ScanSAR and expressed as follows:

$$h_{\ker,az} = \exp\left[-j2\pi \frac{\alpha \cdot r_{sel} \cdot (r_{rot} + r - \alpha r)}{r_{rot}(r_{rot} + r)} f_a t\right] \tag{27}$$

where r_{sel} is the selected reference range. After the azimuth SCFT, the obtained TOPS raw data is expressed as follows:

$$\begin{aligned} S_6(\tau, f_a) &= \mathrm{SCFT}\{s_5(\tau, t) \cdot H_6\} \\ &= C_1 \cdot \mathrm{sinc}\left[\pi K_r \tau_p \left(\tau - \frac{2r}{c}\right)\right] \cdot \mathrm{sinc}\left[\pi \Delta t' \cdot N_{fft}\right. \\ &\quad \left. \cdot \frac{r_{sel} \cdot r_{rot}(r_{rot}+r)}{\alpha(r_{rot}+r-\alpha r)} \left(f_a - \frac{2v^2}{\lambda} \cdot \frac{\alpha(r_{rot}+r-\alpha r)}{r_{rot}(r_{rot}+r)} \cdot \frac{x}{v}\right)\right] \end{aligned} \tag{28}$$

Afterwards, the obtained uniform azimuth space sampling interval for each range is

$$\Delta x = \frac{1}{\Delta t' \cdot N_{fft}} \cdot \frac{\lambda r_{sel}}{2v} \tag{29}$$

Typically, the selected reference range is

$$r_{sel} = \frac{r_{rot}(r_{rot} + r_0)}{\alpha(r_{rot} + r_0 - \alpha r_0)} \tag{30}$$

Additionally, r_{sel} can be changed for the automatic focused TOPS mode SAR image mosaicking in both azimuth and range directions. The SCFT operation in the discrete domain is the chirp-z transform which can be efficiently performed by introducing the FFT codes [20, 25].

4. SIMULATION EXPERIMENT

To validate the proposed imaging algorithm for the TOPS raw data, simulation experiments on point targets are carried out. The simulation parameters are listed in the Table 1. Twelve point targets are placed in the illuminated scene as shown in Figure 5.

It should be noted that the effects on the earth rotation and the yawing control are considered in this simulation. After the yawing control with the angle of 3.8516°, the Doppler centroid of the obtained TOPS SAR raw data is 0.00713 Hz. Figure 6 shows some simulation results after the important processing steps of the proposed imaging algorithm. With the subaperture formulation, the whole raw data

Table 1. Simulation parameters.

Parameters	Value
Carrier frequency	9.65 GHz
Azimuth beam width	0.33°
System PRF	4000 Hz
Transmitted pulse duration	4 μs
Transmitted pulse bandwidth	150 MHz
Sampling frequency	200 MHz
Effective velocity	7200 m
Burst duration	0.32 s
Slant range of imaging center	600 km
Azimuth beam rotation rate	3.415°/s
Angle for yawing control	3.8516°

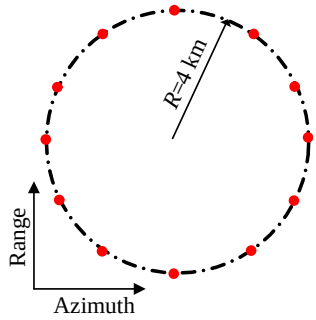

Figure 5. The designed imaged scene with twelve point targets.

of a single burst is divided into six blocks as shown in Figure 6(a), and each block is without the Doppler aliasing problem as shown in Figure 6(b). Simulated raw data in the range-Doppler domain before azimuth scaling by multiplying phase function H_4 are shown in Figures 6(c) and (d), respectively. It can be seen that the aliased Doppler is overcome by introducing azimuth scaling, and the constant factor α in (17) is 0.27 in this simulation. The second azimuth scaling operation removes the azimuth varying beam center time as shown in Figure 6(e). The final focused TOPS SAR image clearly indicates the arrangement of simulated point targets. The processing time of the proposed algorithm is 2.82 s, while the size of the raw data is 1280×13000 (azimuth $\times$ range). With the same case, the processing

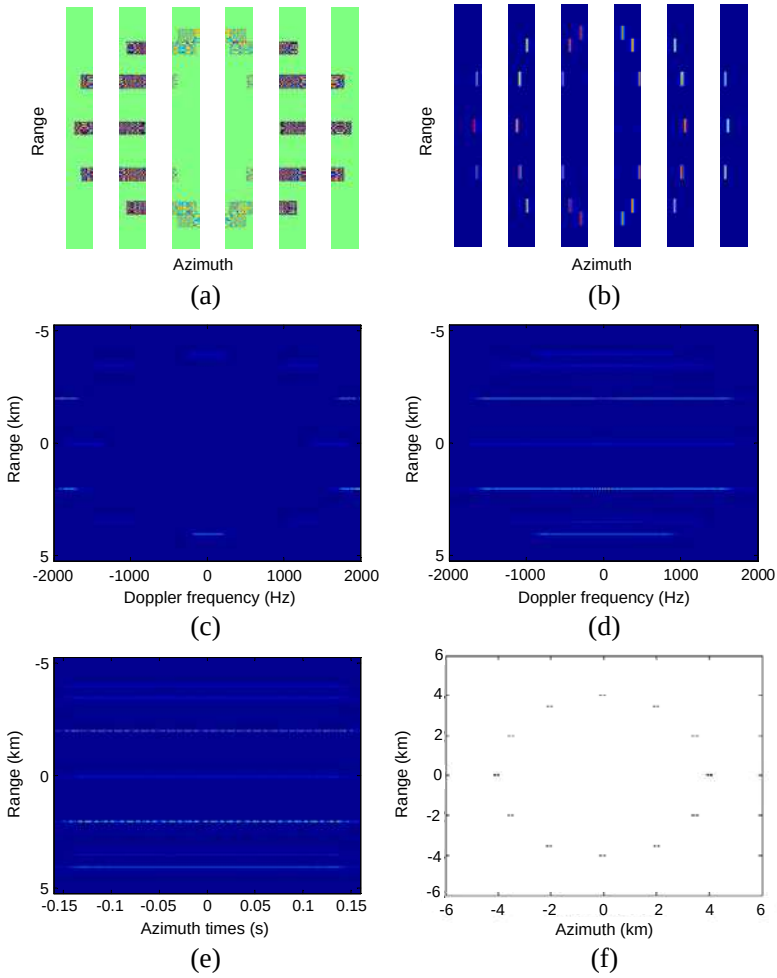

Figure 6. Point array simulation experiment. (a) Subaperture formation in the 2D time domain. (b) Subaperture formation in the range-Doppler domain. (c) Before Doppler centroid varying rate changing. (d) After Doppler centroid varying rate changing. (e) Before the final SCFT operation. (f) The final focused SAR image.

time of algorithms in [1, 5, 9, 10] is 252.16 s, 18.92 s, 53.63 s, 25.32 s, respectively.

To further validate the proposed imaging algorithm and distinguish the limited squinted angles of different point targets, three simulated point targets P_1, P_2 and P_3 with different locations in the

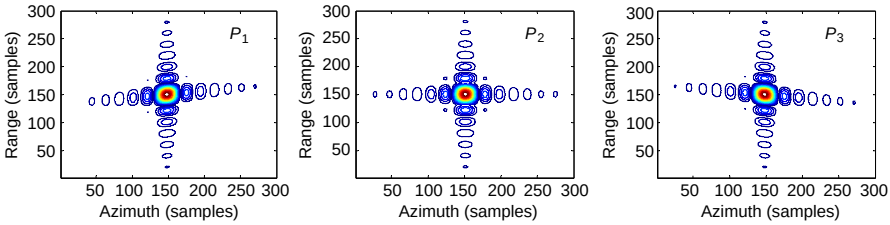

Figure 7. Imaging results of point targets. (a) P_1. (b) P_2. (c) P_3.

Table 2. Simulation parameters.

	Azimuth			Range		
	Res. (m)	PSLR (dB)	ISLR (dB)	Res. (m)	PSLR (dB)	ISLR (dB)
Theoretical	14.28	−13.26	−9.80	0.89	−13.26	−9.80
P_1	14.15	−13.24	−9.96	0.90	−13.28	−10.04
P_2	14.32	−13.26	−10.04	0.89	−13.26	−10.02
P_3	14.58	−13.26	−9.94	0.89	−13.28	−10.02

designed scene are focused. P_2 is located in the imaged scene center, while P_1 and P_3 stay on the border of the designed scene. The relative distance of P_1 in azimuth and in the range direction are −5 km and −10 km, respectively, while the relative azimuth and range distance of P_3 are 5 km and 10 km, respectively. The contour plots of different point targets as shown in Figure 7 present the well focused feature. Imaging parameters of three point targets are computed and listed in Table 2. Moreover, different squint angels of P_1, P_2 and P_3 can be obviously observed.

5. CONCLUSIONS

This paper presents an efficient phase-preserving TOPS mode SAR raw data imaging algorithm based SCFT. In this algorithm, the use of subaperture is adopted to overcome the aliased Doppler spectrum. After RCMC implemented in each azimuth block via the classic CS imaging processor and subaperture raw data recombination, the SPECAN operation is introduced to focus the azimuth signal. Additionally, azimuth scaling and azimuth frequency scaling steps are carried out before the final azimuth SPECAN operation. To obtain the uniform sampling interval for each range bin, conventional Fourier

transform is replaced by the SCFT operator. Simulation on point targets validates the proposed imaging algorithm. Moreover, since the large azimuth data extension and any interpolations are avoided, this algorithm is highly efficient.

ACKNOWLEDGMENT

This work was supported in part by the Research Program of Science and Technology at Universities of Inner Mongolia Autonomous Region under Grant NJZZ11069, in part by the Natural Science Foundation of Inner Mongolia Autonomous Region under Grant 2011BS0904, in part by the National Natural Science Foundation of China under Grant 61201433.

REFERENCES

1. Zan, F. D. and A. M. Guarnieri, "TOPSAR: Terrain observation by progressive scans," *IEEE Trans. Geosci. Remote Sens.*, Vol. 44, No. 9, 2352–2360, Sep. 2006.
2. Xu, W., P. Huang, and Y.-K. Deng, "Multi-channel SPCMB-TOPS SAR for high-resolution wide-swath imaging," *Progress In Electromagnetics Research*, Vol. 116, 533–551, 2011.
3. Xu, W., P. Huang, and Y.-K. Deng, "MIMO-TOPS mode for high-resolution ultra-wide-swath full polarimetric imaging," *Progress In Electromagnetics Research*, Vol. 116, 533–551, 2011.
4. Meta, A., J. Mittermayer, P. Prats, R. Scheiber, and U. Steinbrecher, "TOPS imaging with TerraSAR-X: Mode design and performance analysis," *IEEE Trans. Geosci. Remote Sens.*, Vol. 48, No. 2, 759–769, Feb. 2010.
5. Prats, P., R. Scheiber, J. Mittermayer, A. Meta, and A. Moreira, "Processing of sliding spotlight and TOPS SAR data using baseband azimuth scaling," *IEEE Trans. Geosci. Remote Sens.*, Vol. 48, No. 2, 770–780, 2010.
6. Mittermayer, J., P. Prats, D. D'Aria, R. Piantanida, S. Sauer, A. M. Guarnieri, E. Attema, and P. Snoeij, "TOPS Sentinel-1 and TerraSAR-X processor comparison based on simulated data," *Proc. EUSAR*, 1–4, Aachen, Germany, 2010.
7. Prats, P., L. Marotti, S. Wollstadt, et al., "TOPS interferometry with TerraSAR-X," *Proc. EUSAR*, 44–47, Aachen, Germany, 2010.
8. Xu, W. and Y. K. Deng, "Investigation on electronic azimuth beam steering in the spaceborne SAR imaging modes," *Journal*

of Electromagnetic Waves and Applications, Vol. 25, Nos. 14–15, 2076–2088, 2011.

9. Xu, W., P.-P. Huang, and Y.-K. Deng, "TOPSAR data focusing based on azimuth scaling preprocessing," *Adv. Space Res.*, Vol. 48, No. 2, 270–277, 2011
10. Xu, W., P.-P. Huang, Y.-K. Deng, J.-T. Sun, and X.-Q. Shang, "An efficient imaging approach with scaling factors for TOPS mode SAR data focusing," *IEEE Geosci. Remote Sens. Lett.*, Vol. 8, No. 5, 929–933, Sep. 2011.
11. Prati, C., A. M. Guarnieri, and F. Rocca, "SPOT mode SAR focusing with the ω-k technique," *Proc. IGARSS*, Espoo, Finland, 1991.
12. Lanari, R., M. Tesauro, E. Sansosti, and G. Fornaro, "Spotlight SAR data focusing based on a two-step processing approach," *IEEE Trans. Geosci. Remote Sens.*, Vol. 39, No. 9, 1993–2004, Sep. 2001.
13. Lanari, R., S. Zoffoli, E. Sansosti, G. Fornaro, and F. Serafino, "New approach for hybrid strip-map/spotlight SAR data focusing," *IEE Proc. — Radar Sonar and Navig.*, Vol. 148, No. 6, 363–372, Dec. 2001.
14. Lanari, R., "A new method for the compensation of the SAR range cell migration based on the chirp z-transform," *IEEE Trans. Geosci. Remote Sens.*, Vol. 33, No. 5, 1296–1299, May 1995.
15. Bai, X., J. P. Sun, and W. Hong, "On the TOPS mode spaceborne SAR," *Science China — Information Sciences*, Vol. 53, No. 2, 367–378, Feb. 2010.
16. Bamler, R., "A comparison of range-Doppler and wavenumber domain SAR focusing algorithm," *IEEE Trans. Geosci. Remote Sens.*, Vol. 30, No. 4, 706–713, Apr. 1992.
17. Moreira, A., J. Mittermayer, and R. Scheiber, "Extended chirp scaling algorithm for air- and spaceborne SAR data processing in stripmap and ScanSAR imaging modes" *IEEE Trans. Geosci. Remote Sens.*, Vol. 34, No. 5, 1123–1136, May 1996.
18. Guarnieri, A. M. and C. Prati, "ScanSAR focusing and interferometry," *IEEE Trans. Geosci. Remote Sens.*, Vol. 34, No. 4, 1029–1038, Apr. 1996.
19. Mittermayer, J., R. Lord, and E. Boerner, "Sliding spotlight SAR processing for TerraSAR-X using a new formulation of the extended chirp scaling algorithm," *Proc. IGARSS*, Toulouse, France, 2003.
20. Lanari, R., S. Hensley, and P. A. Rosen, "Chirp z-transform

based on SPECAN approach for phase-preserving ScanSAR image generation" *IEE Proc. — Radar Sonar and Navig.*, Vol. 145, No. 5, Oct. 1998.

21. Wong, F. H. and T. S. Yeo, "An improved technique for the processing of short-dwell spotlight SAR data," *IEEE Trans. Geosci. Remote Sens.*, Vol. 41, No. 5, 953–963, May 2003.
22. Dai, C. and X. Zhang, "Omega-k algorithm for bistatic SAR with arbitrary geometry configuration," *Journal of Electromagnetic Waves and Applications*, Vol. 25, Nos. 11–12, 1564–1576, 2011.
23. Guo, D., H. Xu, and J. Li, "Extended wavenumber domain algorithm for highly squinted sliding spotlight SAR data processing," *Progress In Electromagnetics Research*, Vol. 114, 17–32, 2011.
24. An, D. X., Z.-M. Zhou, X.-T. Huang, and T. Jin, "A novel imaging approach for high resolution squinted spotlight SAR based on the deramping-based technique and azimuth NLCS principle," *Progress In Electromagnetics Research*, Vol. 123, 485–508, 2012.
25. Wu, J., Z. Li, Y. Huang, Q. H. Liu, and J. Yang, "Processing one-stationary bistatic SAR data using inverse scaled fourier transform," *Progress In Electromagnetics Research*, Vol. 129, 143–159, 2012.